Icarus 317 (2019) 94–103

Contents lists available at ScienceDirect

Icarus

journal homepage: www.elsevier.com/locate/icarus

Dynamical processes of dust lifting in the northern mid-latitude region of Mars during the dust storm season☆

Xiao Jing, Chow Kim-Chiu*, Chan Kwing-lam

Space Science Institute / Lunar and Planetary Science Laboratory, Macau University of Science and Technology, Administration Building, Block A, Avenida Wai Long, Taipa, Macau

ARTICLE INFO

Keywords:
Mars
Dust storms
Mid-latitude waves
Wavelet analysis
Topography

ABSTRACT

The general circulation model MarsWRF has been used to simulate the regular dust climate on Mars. In particular, the double-peak episodes of dust storm activities during the dust storm season can be captured with the use of an active dust lifting scheme in the model. This study focuses on the dynamical processes of dust lifting in the northern mid-latitude region during these episodic periods. Wavelet analysis to the time series shows that dust lifting activities are associated with three distinct modes of variability. The first is the high frequency signal with a period of 0.5 to 1 sol, which is generally associated with the thermal tide. The second mode has the period about 7 sols, which is generally associated with the mid-latitude planetary waves. The third mode has the period over 50 sols, which is basically the signal of seasonal change in the region. Further analysis on wave numbers suggests that the dust lifting processes are dominated by the mode around wave number three. Results of sensitivity experiments also suggest that topography in the northern mid-latitude region is important to the lifting of dust in the period around 1 sol.

1. Introduction

Previous observations (e.g., Montabone et al., 2015; Kass et al., 2016) show that the regular annual activity of Martian dust storms is concentrated in the second half of the Martian year (solar longitude Ls = 180 - 360°). However, even in this period of "dust storm season", dust storms are not prevailing all the time but are more active in two episodic periods (Ls = 220° - 260° and Ls = 310° - 340°). Between these two periods dust storms are significantly less. This double-peak occurrence of dust storms with a quiet period in between has been identified in some observational studies and is usually referred as the "solsticial pause" (e.g., Wang and Richardson, 2015; Kass et al., 2016; Lewis et al., 2016).

During the double-peak episodes, relatively frequent occurrence of dust storms can be observed over the northern mid-latitude region (e.g., Cantor et al., 2001; Wang, 2007; Guzewich et al., 2015; Lemmon et al., 2015; Wang and Richardson, 2015). In fact, Hollingsworth et al., (1996) has suggested that a storm zone as on Earth can also be identified on Mars. From these previous studies (e.g. Hollingsworth et al., 1996), the favorite originating regions include the Acidalia region, followed by the Utopia and Arcadia regions. In particular, the dust storms initiated over Acidalia are far more than the others (Wang and Richardson, 2015; Hinson et al., 2012; Guzewich et al., 2015). These three regions are all located downstream of three high topographic regions of Alba Patera, Syrtis Major and Elysium. In some occasions, the initiated dust storms may "flush" southward and cross the equator, and may strengthen again in the southern hemisphere (Cantor et al., 2001; Wang et al., 2003, 2005; Wang 2007). This southward transport of "flushing storms" would help distribute the dust to the southern hemisphere, and also affect the general circulation.

The frequent occurrence of dust storms over the northern mid-latitude region during the dust storm season has been suggested to be related to the transient mid-latitude wave activities (e.g. Barnes, 1980; Hinson and Wang, 2002; Banfield et al., 2004; Hollingsworth and Kahre, 2010; Kass et al., 2016). Therefore, many previous studies have been devoted to investigate the characteristics of these waves (e.g., Wang et al., 2005; Kuroda et al., 2007; Kavulich et al., 2013; Hinson and Wang, 2010; Hinson et al., 2012; Wang et al., 2013; Wang and Toigo, 2016). In the studies, wavelet or spectrum analysis were mainly focused on the zonal decomposition of the signals, and the results generally suggest that the dominant zonal wave number of the waves is 2 to 3 with the dominant period between 2 to 4 sols during the double-peak episodic periods of dust events, while they are suppressed during the solstice period. The dominated waves during the solsticial pause

☆ Revised in July 2018.

* Corresponding author.
E-mail address: kcchow@must.edu.mo (K.-C. Chow).

https://doi.org/10.1016/j.icarus.2018.07.020
Received 27 April 2018; Received in revised form 1 July 2018; Accepted 25 July 2018
Available online 27 July 2018
0019-1035/

have a zonal wave number 1 with the period of 6 to 7 sols and are located at higher altitudes (Read and Lewis, 2004; Kuroda et al., 2007; Hinson and Wang, 2010; Read et al., 2011; Hinson et al., 2012; Wang and Richardson, 2015; Wang and Toigo, 2016; Lewis et al., 2016). Furthermore, some previous studies (e.g., Hinson and Wilson, 2002, Banfield et al., 2004) suggest that the strongest waves during the storm season (dominated by zonal wavenumber 2 ~ 3) are generally more significant in the lower level of the atmosphere, which may result in perturbations of the low-level temperature (up to ~7 K) and wind speed (10 - 15 ms^{-1}).

Since most observations show a high correlation between planetary wave activities and dust storms (e.g., Hinson et al., 2012), the above mentioned previous studies have focused more on planetary wave activities, particularly the zonal wave numbers. On the other hand, the processes of dust lifting with short period in the scale around one sol were generally not considered. This may be due to two reasons. First, most of these observations are based on remote sensing in Sun-synchronous orbits (such as MGS and MRO, Montabone et al. 2015), and so the temporal resolution are limited (no more than two times per day) at one location. As a result, some dust lifting process with short time scales might not be detected. Second, many previous numerical studies used the prescribed dust approach (actually the optical depth) to realistically simulate the observed general circulation (e.g., Kuroda et al., 2007; Mulholland et al., 2016), which is generally not well simulated by using the approach of active dust parameterizations. Although dust lifting processes with short time were usually not considered, their importance should not be ignored. In one recent simulation study by using a Mars GCM (with active dust parameterization), Hollingsworth and Kahre (2010) show that dust can be lifted by the nocturnal down-slop winds over the Tharsis volcanoes and Alba Mons, and then transported to the downstream regions along with the transient frontal systems.

The present study focuses more on the dynamics pertinent to dust lifting, and the analysis is mainly on the dynamics near the surface. In addition, the effect of asymmetric topography in the northern mid-latitudes on the waves and dust lifting has been investigated. In this study, the general circulation model MarsWRF with active dust parameterization scheme is used to study the characteristics of the northern mid-latitude waves pertinent to dust lifting. In Section 2, the numerical model used in this study and the basic configurations of the simulations will be introduced. The dynamic processes contributed to the mid-latitude dust storms simulated by the model will be analyzed and discussed in Section 3. The effect of the northern mid-latitude topography on the waves and dust lifting will be discussed in Section 4, and the results of this study will be summarized and discussed in Section 5.

2. The numerical simulations

The general circulation model (GCM) MarsWRF has been used in this study, which is developed from the widely-used WRF model for Earth's weather research and forecasting (Skamarock and Klemp, 2008). MarsWRF is basically the Mars version of the PlanetWRF model (Richardson et al., 2007), and has been illustrated in Richardson et al. (2007) and Toigo et al. (2012) that it is capable of realistically reproducing most climate features such as the large-scale general circulation and temperature field on Mars. The basic configuration of the simulations is generally similar to that used in Chow et al., (2018), as described in the following. The global domain of the model has 36 latitude × 72 longitude grid points (horizontal spatial resolution of about 5° or 300 km in the equatorial region). There are 52 vertical levels in terrain-following hydrostatic-pressure vertical coordinate (Skamarock and Klemp, 2008), and the model top is set at 0.0057 Pa (about 80 km in altitude). Half of these 52 levels are located between the model top and the pressure level of 100 Pa. Non-hydrostatic dynamics is used for the model runs and the damping flag at upper levels is turned off. The 3rd order Runge-Kutta scheme is adopted for the time-integration. The advections of momentum and scalar variables have 5th order and 3rd order accuracy in the horizontal and vertical directions respectively. To deal with the turbulence and mixing processes, the 2nd order diffusion terms are evaluated on coordinate surfaces and the eddy coefficient is given by the horizontal Smagorinsky first order closure theory. In addition, some other filters like the divergence damping and external-mode filter are applied with typical strength.

The physical processes chosen in the simulations are suitable for the Martian environment. The radiation scheme for short- and long-wave radiation employed in these simulations is the "wide band model" scheme as described in Richardson et al. (2007), Toigo et al. (2012) and Newman and Richardson (2015). This scheme considers the heating/cooling effects of dust and the phase change of carbon dioxide (CO_2). The planetary boundary layer scheme and land surface scheme were largely adapted from existing terrestrial schemes in WRF (see Richardson et al., 2007 and Toigo et al., 2012). In particular, the friction velocities and exchange coefficients are calculated by the WRF SFCLAY Monin–Obukhov surface-layer scheme (Jiménez et al., 2012), which are then used to calculate the heat and moisture fluxes by the land-surface and boundary-layer models. The Martian 12-layer subsurface diffusion scheme is used as the land-surface model and the Medium Range Forecast Model (MRF) boundary layer scheme is employed to deal with an unstable boundary layer (Hong and Pan, 1996). The model also includes other physical process parameterizations specific to Mars, such as the carbon dioxide cycle (Guo et al., 2009) and the dust lifting process (Newman and Richardson, 2015). However, no parameterization of the water cycle is included in these simulations.

The parameterization of dust processes in the model includes two interactive dust schemes similar to those used in Newman and Richardson (2015), and dust is assumed to be available everywhere and at all times over the whole planet surface except those surfaces with ice cover. The first scheme is similar to some usual dust models on Earth, in which the lifting of dust is proportional to the surface wind stress. Dust lifting occurs over the surface when the local near-surface stress exceeds a particular threshold value (constant value 0.043 N m^{-2} in this study). The second scheme provides most of the background dust, which is parameterized as dust lifting by dust devils. The amount of dust lifting is dependent on the temperature difference between the surface and the air above, as well as the sensible heat flux. The radiation scheme in the model is interactive with dust so that the suspended dust may change the atmospheric radiation and thus the circulation. Dust particle size may have important effect on the radiation and dust sedimentation processes. In this study, the model considers dust particles have two sizes of 1 and 2 μm. The averaged mixing ratio of these two kinds of dust particles is considered as the mixing ratio of the dust particles in the atmosphere. In general, the parameters in the two-size dust lifting schemes are adjusted to simulate the observed dust climatology.

The model was run for two Martian years, initially starting from the time of northern spring equinox (L_S = 0°), and the output interval is 2 h. The first year is considered as the spin up period. For the analysis of dust lifting dynamics discussed in the following sections, the simulation result of the second year of model run is considered. This single-year model run will be referred as the control experiment (CTRL) hereafter.

The vertical profiles of temperature and zonal wind (Fig. 1) from CTRL suggest that the model is capable of simulating the regular dynamic field of Mars during the solstice period (L_S = 265° - 275°). The temperature profile (Fig. 1a) has the maximum (over 240 K) near the surface in the middle to high latitude region in the southern hemisphere, while the minimum temperature (less than 140 K) is located at the altitude about 40 km near the north pole. The warm and cold polar air masses establish a strong meridional temperature gradient region in the latitudes between 30° to 70° N. The gradients are tilting northward with height similar to the polar front on the Earth. Corresponding to the thermal field, the global circulation contains a cross-equatorial overturning cell stretching from 60° S to 45° N, and a westerly jet (maximum

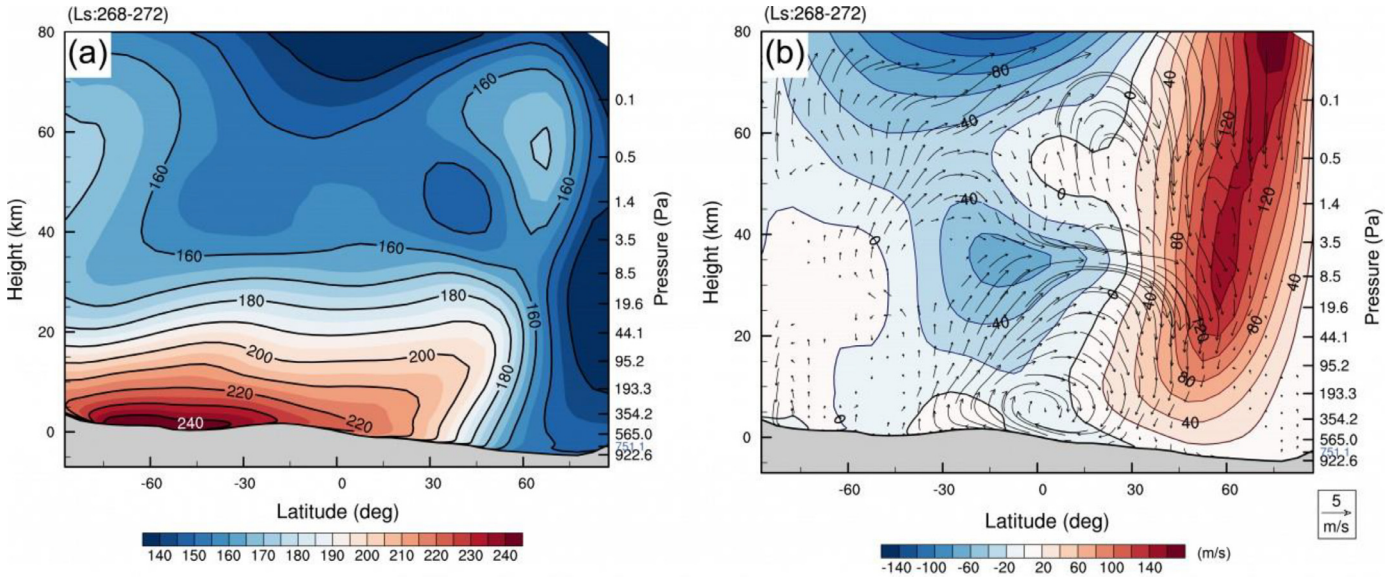

Fig. 1. Vertical profiles of simulated zonal-mean thermal and dynamic variables averaged around the solstice point (L_S = 265° - 275°). (a) Temperature (contours and shaded, K); (b) zonal wind speed (contours and shaded, ms^{-1}) and the meridional-vertical circulation (vertical component × 100, and only vectors with magnitudes > 0.25 ms^{-1} are shown).

zonal wind speed exceeds 160 ms^{-1}) near the front (Fig. 1b). Overall, the simulated thermal and dynamical structures in the model climatology are fundamentally similar to the observations (e.g., McCleese et al., 2010; Heavens et al., 2011) and GCM simulations (e.g., Basu et al., 2006; Richardson et al., 2007).

As in Chow et al. (2018), the model simulation in CTRL could also reasonably capture the pattern of the observed annual variation of Martian dust activities. The solar longitude-latitude evolution of the simulated zonal-mean column dust optical depth (CDOD) normalized to 700 Pa (Fig. 2a) is generally similar to the observed climatology of dust on Mars (Montabone et al. 2015). The dust lifting activities show two prominent episodic periods in Ls = 220° - 260° and Ls = 310° - 340°, corresponding to the cold season in northern hemisphere. In the simulations, dust storms are usually initiated in the mid-latitudes (around 45° N) and some of them may move southward and cross the equator

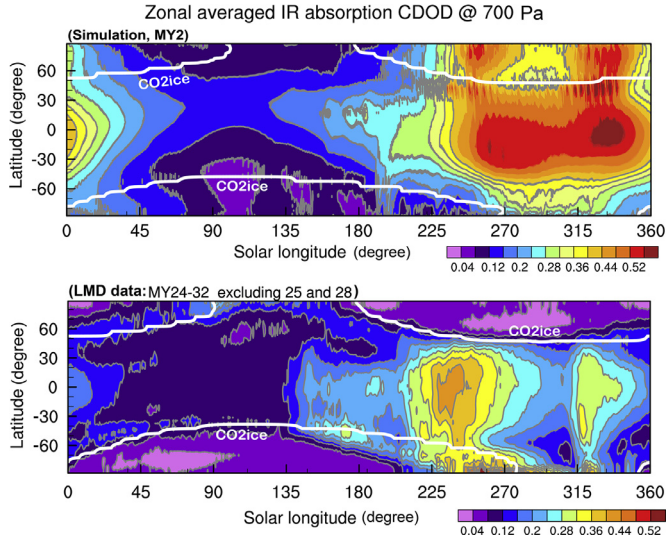

Fig. 2. Annual variation of zonal-mean column dust optical depth at 9.3 μm (normalized to 700 Pa surface) from the model simulation (upper panel) and the re-constructed observational data (Montabone et al., 2015) averaged for the six Martian years without global-scale dust storms (lower panel). White contours depict the corresponding CO_2 ice cap edges.

(flushing storms discussed in Wang and Richardson, 2015). During the solstice period (Ls = 270° - 310°), dust storms in the northern hemisphere are suppressed, but dust storms still exist in the south polar region (Fig. 2a). This suppression is usually called the "solsticial pause" of dust activities (e.g., Wang and Richardson, 2015; Kass et al., 2016; Lewis et al., 2016). It is worth mentioning that there is a certain bias of dust distribution simulated in CTRL. For instance, there is some excessive dust simulated in the equatorial region as well as in the northern polar region, while there is insufficient dust near the CO_2 cap edge in the southern hemisphere.

For the discussions in the following sections, it is also worth to show the spatial distribution of daily maximum dust mixing ratio (Fig. 3) simulated in CTRL. The distribution may reflect the source regions of dust storms during the dust storm season. In the northern hemisphere, the source regions are mainly located between 40° - 50° N, particularly in the north and downstream of three regions with relatively high terrain (Alba Patera, Acidalia and Elysium Mountains). This distribution is similar to the observed maximum optical depth during Ls = 220° - 230° in Martian Year 24 (e.g. Figs. 5 and 8 in Wang and Richardson, 2015). In the following discussions, the mid-latitude region refers to the region with latitudes between 42.5° and 47.5° N.

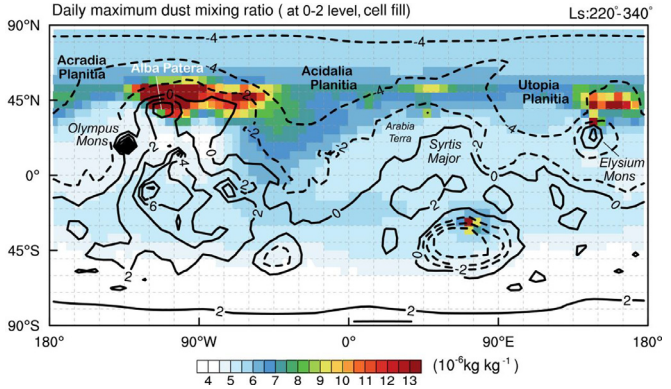

Fig. 3. Distribution of the simulated daily maximum dust mixing ratio (shading, 10^{-6} kg kg^{-1}) near the surface (0–2 levels) averaged over the period of Ls = 220° - 340°.

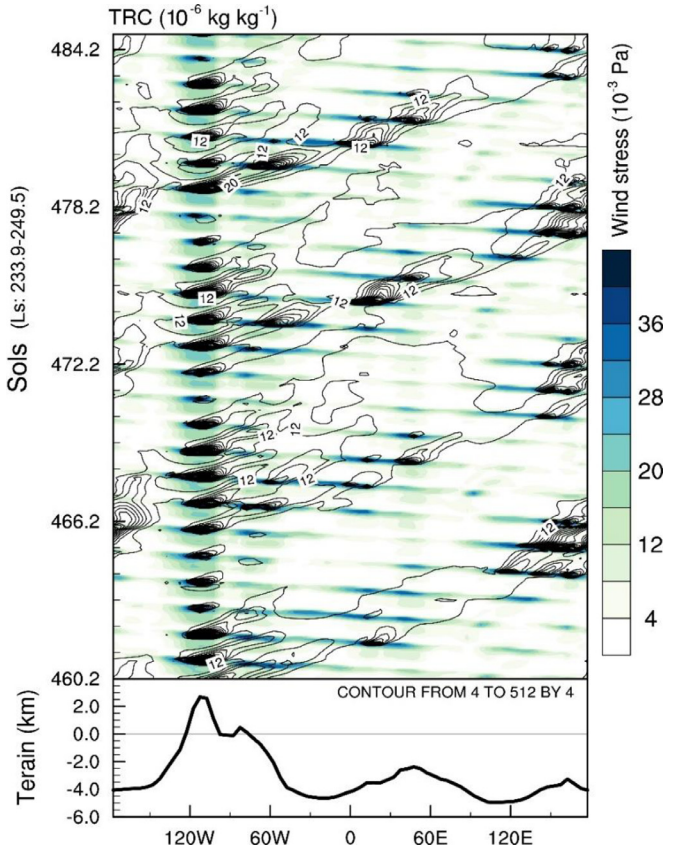

Fig. 4. Hovmöller diagram of surface dust mixing ratio (contours, 10^{-6} kg^{-1}) and wind stress (shading, 10^{-3} N m^{-2}) averaged between 42.5° and 47.5° N during sols 460.2 - 484.2 (Ls = 233.9° - 249.5°). The corresponding profile of terrain (km) in the region is shown in the bottom.

3. Dust lifting processes in the simulations

3.1. Characteristics of dust lifting activities

To investigate the characteristics of dust lifting activities during the episodic period, in this section, the results from the control experiment (CTRL) will be analyzed for the period between Ls = 233.9° and 249.5°. The variations of the zonal-mean surface dust mixing ratio and wind stress in the northern mid-latitude region (Fig. 4) shows that the dust lifting activities may involve a multi-frequency process. It appears that the surface stress is usually amplified over three regions with high topography (120°～100° W, 30°～60° E, 150°～180° E; corresponding to the regions of Alba Patera, Arabia Terra and Elysium Mountain, respectively), particularly over the region of Alba Patera (～ 120° W). The frequency of the signal is relatively high (approximately once per sol) and shows a westward propagation. The increase in dust mixing ratio is generally corresponding to the increase in surface stress (Fig. 4), and hence dust lifting is mainly active over the above mentioned three regions with high topography. However, unlike the surface stress, the signal of dust lifting appears to have an eastward propagation with a lower frequency (～ 6 sols). It is also worth pointing out that dust lifting occurs over the Alba Patera for almost every sol but it is generally not the case in the other two regions.

To further analyze the above multi-frequency process of dust lifting, wavelet analyses have been done on the time series of the results over the mid-latitude region (Fig. 5). In these analyses, instead of considering the time series of the zonal-mean variables, we consider the time series of the results averaged over the longitude band between 120° W and 0° W. This band refers to the region of the Alba Patera. Compared with the zonal-mean results, the signals in the analyses are generally clearer for the results in this band. It can be shown that the patterns of the signals in the analyses using the zonal-mean results are generally similar (figures not shown).

The wavelet analysis of the low-level (averaged between 0–2 levels, and the same hereafter) dust mixing ratio (Fig. 5a) indicates that three significant (> 95%) discrete time scales above the e-folding line can be identified, named in this study as the diurnal scale (0.5 to 1 sol), synoptic scale (3 to10 sols) and seasonal scale (50 to 200 sols). The wave energy of the first two scales is most significant during the dust storm season, and solsticial pauses in the signals are generally present (also see the lower curves in Fig. 5a). The corresponding wavelet analysis of the surface wind stress (Fig. 5b) shows the similar time scales as for the low-level dust mixing ratio, except that the synoptic and seasonal scales (～120 sols) of variation are much weaker than the diurnal time scale (Fig. 5b).

To support the findings mentioned above, it is worth considering a similar wavelet analysis using the results from the reanalysis data Mars Analysis Correction Data Assimilation (MACDA v1.0), which is publicly available from the Centre for Environmental Data Analysis (Montabone et al., 2014). From the wavelet analysis of the surface wind speed of the MACDA data (Fig. 5c), it also shows these three distinct time scales of variations and support the simulation result.

3.2. Dynamics of dust lifting

The wavelet analyses in Section 3.1 suggest that three time scales can be identified in the time series of the variables related to the dust lifting activities. In this section, the dynamics of the processes corresponding to these three time scales will be analyzed and discussed.

a. Diurnal scale process (0.5–1 sols)

It has been discussed above that the diurnal scale variations of low-level dust and surface stress (Fig. 4) are very significant, particularly over the Alba Patera. To investigate the dynamics of dust lifting in this diurnal scale, the corresponding evolution of the surface wind vectors are considered (Fig. 6). It can be seen that regions with high surface wind stress (shading in Fig. 6) are basically organized in a belt shape, showing the propagation from east to west. The propagation is basically consistent with the westward propagation of the maximum solar radiation, suggesting the process on this time scale is likely associated with the thermal tides. The regions of high surface stress are mainly near the three regions with high topography as discussed before, and are generally corresponding to evolution of the surface wind vectors (red vectors in Fig. 6). The surface winds in these three regions are mainly southerly in direction, but apparently turn into westerly when there is an elevated surface stresses.

The evolution of the surface wind vectors suggests that the three high terrain regions may enhance the westerly winds associated with the elevated surface stresses, which turns out the lifting of dust if the threshold stress is exceeded there. The associated dynamical process can be further investigated by considering the diurnal evolution of thermal and dynamical fields (Figs. 7 and 9). Due to the relatively small thermal inertia of the land surface on Mars, increase in ground temperature due to solar short wave radiation is dramatic (Fig. 7 b1 - b4 shading) and presenting a prominent diurnal cycle (Fig. 8 red line). During the cold season of the northern hemisphere, the solar radiation is decreasing rapidly northward in the mid-latitude region, and so do the ground temperature and low-level geopotential height. As a result, the maximum meridional gradients of temperature and low-level geopotential height occur about the local noon at 45° N, especially near the northern flanges of the mentioned three high terrains (Fig. 7b1-b4). The wind fields are finally turned into westerly and intensified due to geostrophic adjustment (Fig. 7a1-a4, Fig. 8). Therefore, dust storms could be triggered to form near the northern flanges of the three high terrains during the local noon. It is worth noting that the surface air density drops as the ground temperature increases, and so the wind

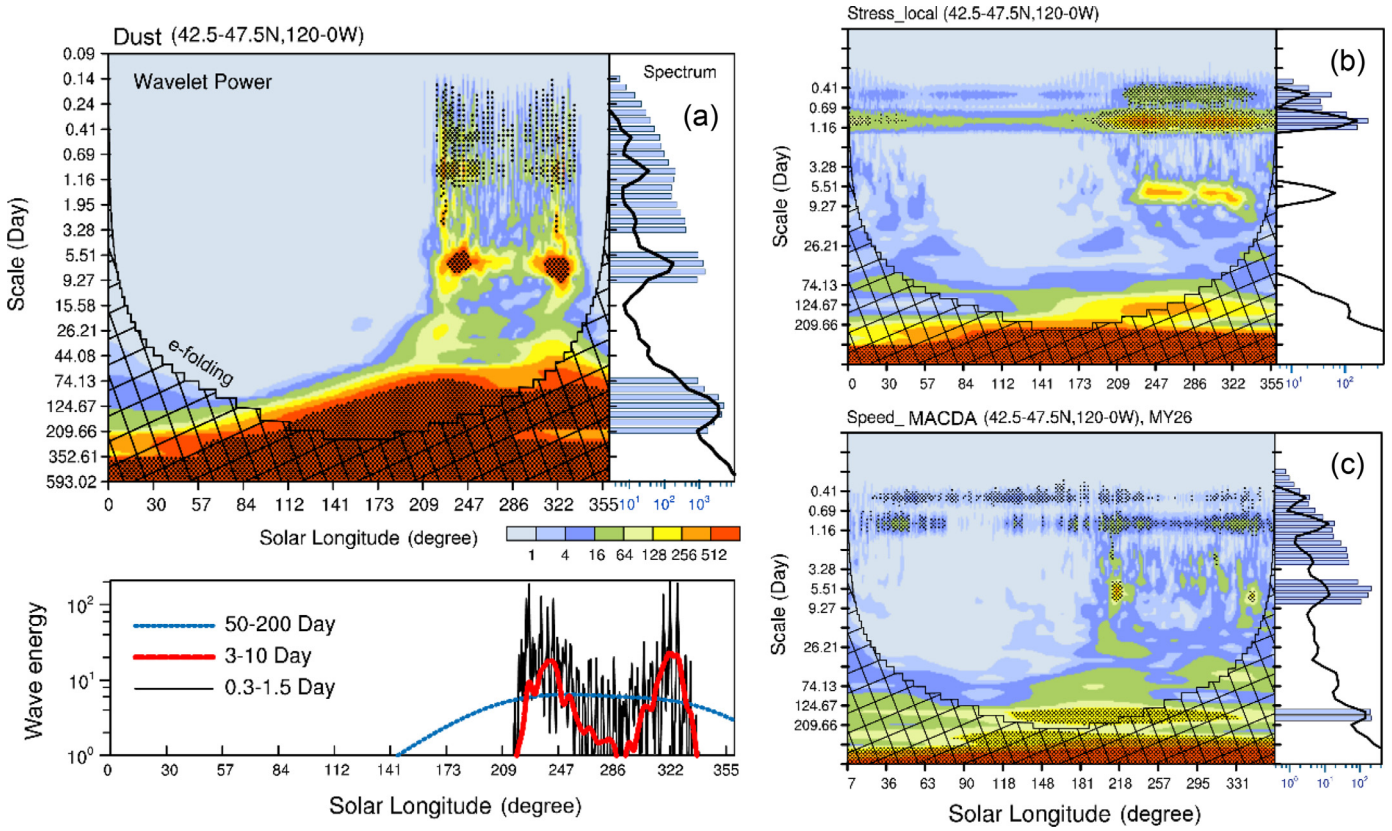

Fig. 5. Wavelet analysis on the time series of some variables averaged in the mid-latitude region near Alba Patera (42.5° - 47.5° N and 120° - 0° W). (a) Simulated dust mixing ratio near surface; (b) simulated surface wind stress; (c) surface wind speed in MY26 from MACDA data. In each sub-figure, the shading depicts the spectrum power (significant region is dotted and the mesh marks where it is above the e-folding line), and the time-averaged spectrum is shown in the upper right (curve is the total energy profile and bars are the effective energy). The panel in the bottom left shows the time series of wave energy of the interested wave bands in (a).

stress gets its maximum a little earlier than the meridional gradient of geopotential height does (Fig. 8). There also presents a secondary wind stress maximum during the local middle night when the air density is at a higher level (Fig. 8), corresponding to the quasi-stationary high southerly wind region shown in Fig. 6.

b. Synoptic scale process (3–10 sols)

Although the diurnal process of dusting lifting is significant in regions with high terrain, the dust lifting activities over the Acidalia and Utopia are apparently dominated by a lower frequency process with period about 6 sols (Fig. 4). To investigate the process of dust lifting on the synoptic time scale, we consider the corresponding Hovmöller diagram (Fig. 9a) for the daily-mean results (diurnal variations are removed). Without the diurnal variation, the low-level dust and the associated surface wind stress show a clear eastward propagation with nearly constant frequency and velocity (Fig. 9a). These waves take 6 to 7 sols to circle around the planet in the mid-latitude region, and could survive for more than one circle. The amplitudes of the waves also show an enhancement over the three regions with high terrain (Fig. 9a), resulting in an apparently zonal wave number three feature. This can be confirmed by considering the spectrum analysis of the daily-mean surface stress in the zonal direction (Fig. 9b), which shows that the synoptic scale process is dominated by a wavenumber around 3, and the spectrum energy extends to wavenumber 10 during the whole dust storm season. The result in this study is consistent with some previous observational and numerical studies (e.g., Wang et al., 2005; Kuroda et al., 2007; Kavulich et al., 2013; Hinson and Wang, 2010; Hinson et al., 2012; Wang et al., 2013; Wang and Toigo, 2016), which found that the mid-latitude waves are dominated by the zonal wave number of two or three.

The relationship between the diurnal and synoptic processes can be further analyzed by considering the time series of low-level dust mixing ratio at the three regions with high topography (Fig. 10). In the Alba Patera region (120° - 100° W), dust lifting apparently occurs at nearly the same time of every sol but appears to be stronger for every 6 to 7 sols. These 6 to 7-sol period of dust episodes appear to be associated with the subsequent events of dust lifting (eastward propagations indicated by the grey bars) in the other two regions of Syrtis Major (30° - 90° E) and Elysium Mons (150° - 180° E). In these two regions, dust lifting is usually not active for every sol but at a period of 6 to 7 sols. It is speculated that this synoptic scale process of dust lifting is associated with the mid-latitude waves initiated from barotropic and/or baroclinic instability in the mid-latitude region (e.g., Read et al., 2015).

c. Seasonal scale process (50–200 sols)

Dust lifting is basically dependent on surface wind stress which turns out to be dependent on the surface wind speed. When the cold season is approaching in the northern hemisphere, the mean westerly wind in the mid-latitude region is increasing due to the seasonal change of the Hadley circulation. This seasonal increase in the mean westerly wind would be the basis for the processes of dust lifting on the seasonal time scale (Fig. 5) as discussed in Section 3.1.

4. Effects of topography

As discussed in the previous section, Martian dust storms during the dust storm season are usually initiated over the three regions with high terrain, particularly the northern flange and lee sides of the mountains in these regions. To investigate the effect of the northern mid-latitude topography on the characteristics of the dust lifting processes discussed before, a sensitivity experiment named RmTerrain has been conducted in which the zonal asymmetry of the terrain has been removed. In this

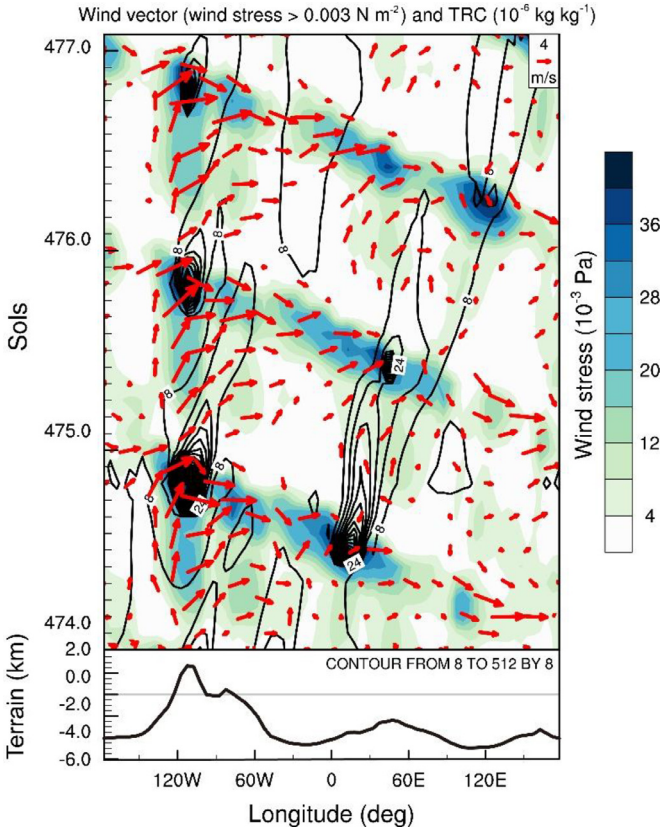

Fig. 6. Similar to Fig. 4 but for the period of sols 474 - 477. Shown together are the corresponding surface winds (vectors) when wind stress is significant ($> 0.003\,\mathrm{N\,m^{-2}}$).

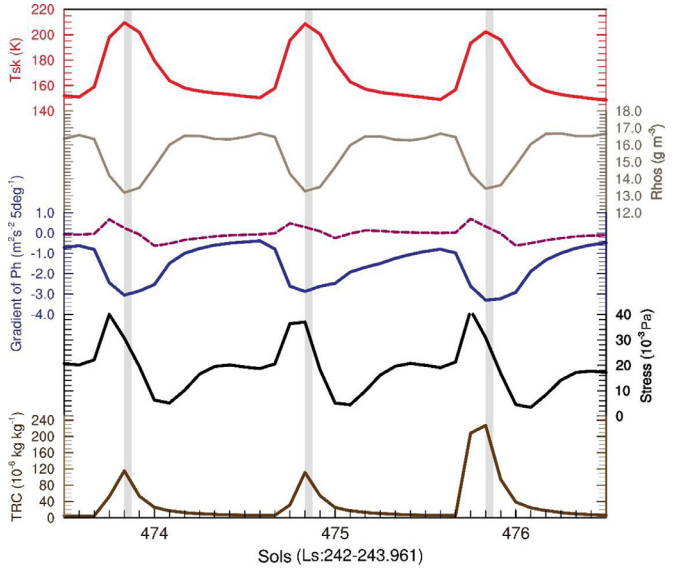

Fig. 8. Diurnal variations of some simulated variables averaged in the mid-latitude region near the Alba Patera (42.5°- 47.5° N, 120°- 100° W) during the period of sols 473.5 - 476.5. The variables shown are the skin temperature T_{sk} (red curve, K), surface air density Rhos (grey curve, $\mathrm{gm^{-3}}$), gradients of geopotential height PH in the east-west direction (purple curve, $\mathrm{m^2s^{-2}}$/grid length) and in the south-north direction (blue curve, $\mathrm{m^2s^{-2}}$ / grid length), surface wind stress (black curve, 10^{-3} Pa) and mixing ratio of the tracer (dust) TRC at the two lowest levels (dark tan curve, $10^{-6}\,\mathrm{kg\,kg^{-1}}$). (For interpretation of the references to color in this figure legend, the reader is referred to the web version of this article.)

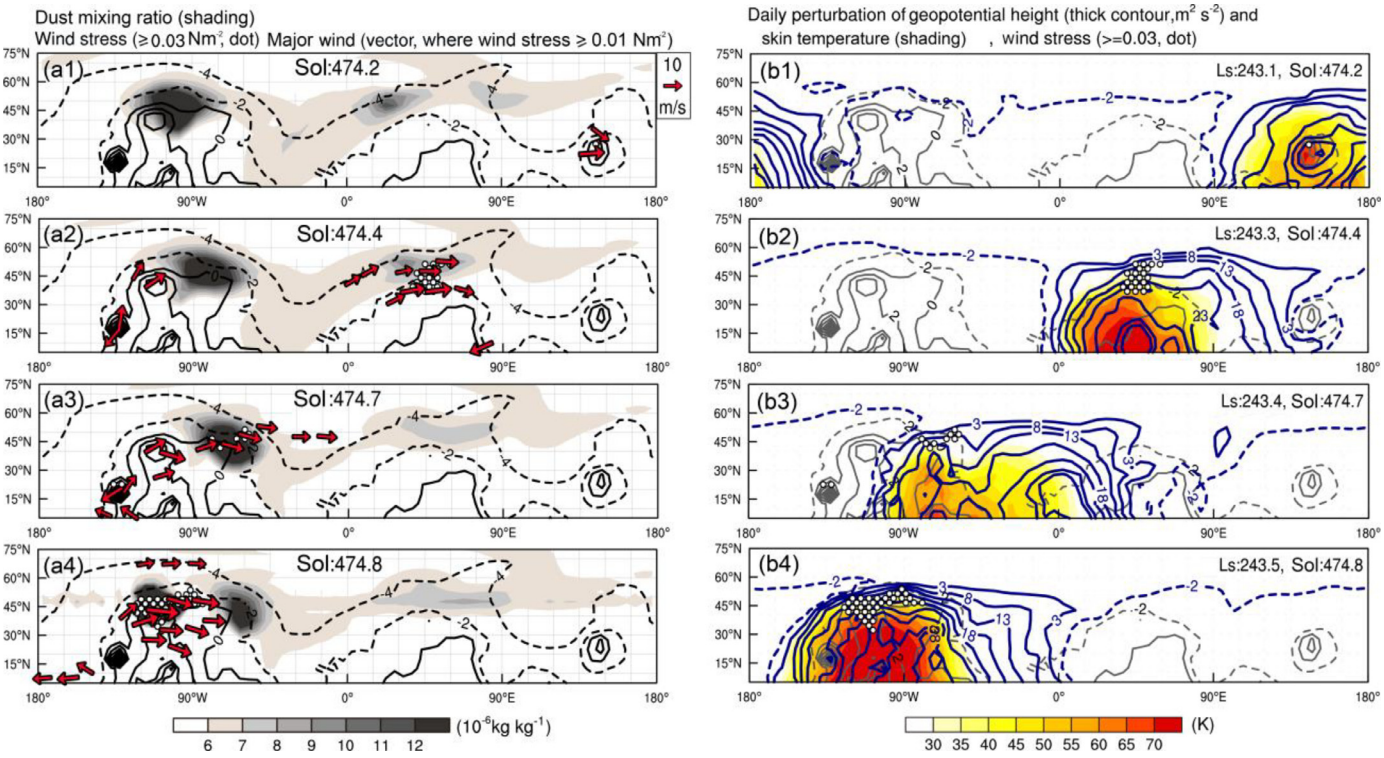

Fig. 7. Diurnal evolution of dust and dynamical-thermal fields. (a1) - (a4) Dust mixing ratio at the lowest two levels (shading, unit: $10^{-6}\,\mathrm{kg\,kg^{-1}}$), major wind vectors (where the wind stress $\geq 0.01\,\mathrm{N\,m^{-2}}$). (b1) - (b4) Daily perturbation of surface air temperature (shading, K) and geopotential height (blue contours, $\mathrm{m^2s^{-2}}$). Rows 1 to 4 are corresponding to sols 474.2, 474.4, 474.7, 474.8 respectively. Black contours indicate the topography (km) and areas with large surface wind stress ($\geq 0.03\,\mathrm{N\,m^{-2}}$) are dotted. (For interpretation of the references to color in this figure legend, the reader is referred to the web version of this article.)

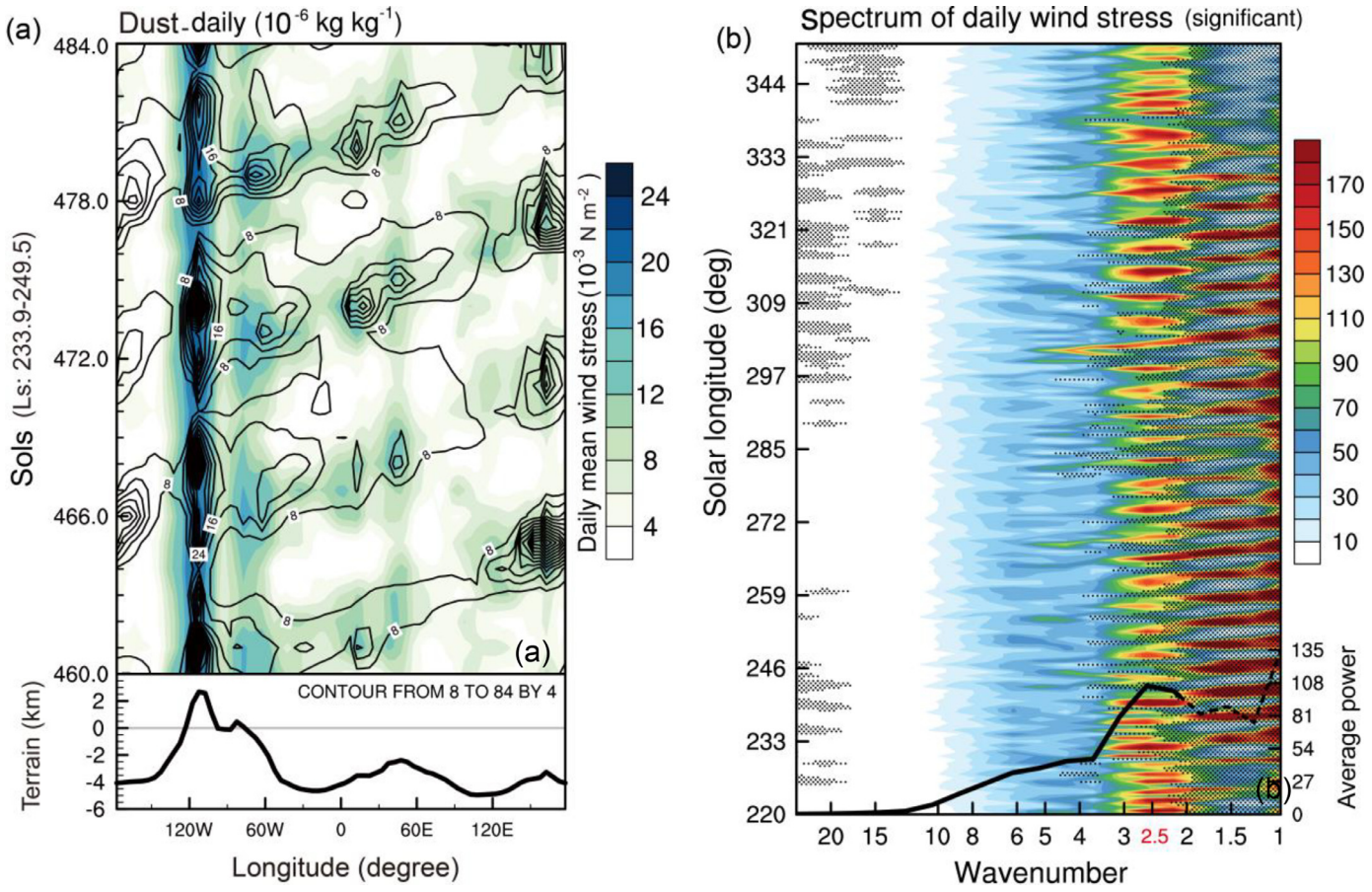

Fig. 9. Analysis of some simulated daily-mean variables. (a) Hovmöller diagram similar to Fig. 4 except for the corresponding daily-mean variables. (b) Time evolution (Ls = 220°- 350°) of wave spectrum (shading, the insignificant regions are dotted, unit = 1) of daily mean surface wind stress that averaged between 40° and 50° N. The black curve depicts the spectrum power averaged over the period.

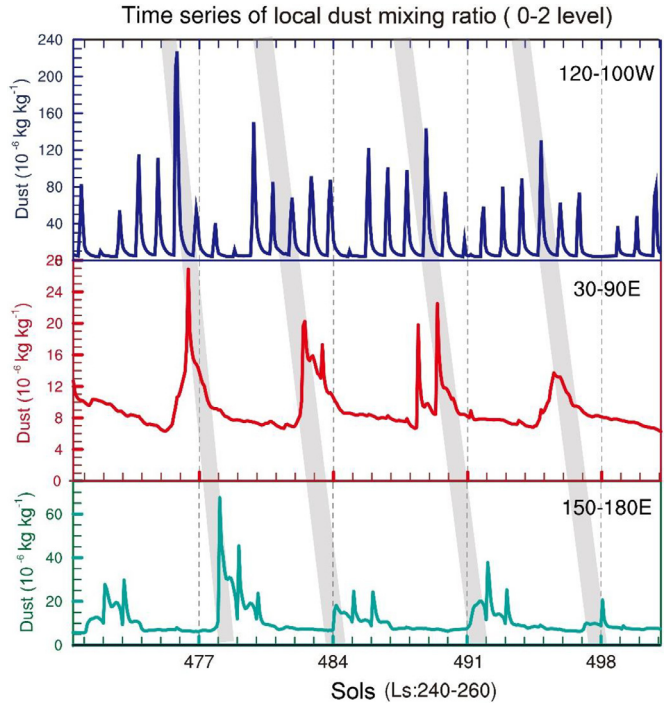

Fig. 10. Time series of surface dust mixing ratio (10^{-6} kg kg^{-1}) in the three regions: Alba Patera (120° − 100° W, Top), Syrtis Major (30° − 90° E, Middle) and Elysium Mons (150° − 180° E, Bottom).

experiment, the original terrain north of 15° N was replaced by the zonal-mean value with 9-point smoothing, while the thermal inertial coefficient and surface roughness are keeping unchanged. In this configuration, the high mountains in the northern mid-latitudes such as the Alba Patera, northern Syrtis Major, Elysium Mons, and even the Olympus Mons (the highest mountain on Mars, south-west to Alba Patera) have been smoothed off (Fig. 11).

The results of RmTerrain suggest that the high terrain in the northern mid-latitudes is important to the dust lifting activities in the region (Fig. 12). Without the zonal asymmetry of topography in the northern mid-latitudes, dust optical depth could be decreased significantly in nearly the whole planet (Fig. 12a) except for the two dust bursts near the south pole during Ls = 270° and Ls = 300° to 315°. In particular, the double-peak episodes of dust events around 45° N apparently disappeared. The effect of topography can be further analyzed by comparing the time series of zonal-mean dynamic and thermal fields in the northern mid-latitude region from the two experiments (Fig. 12b1 - b2). In CTRL, the low-level dust mixing ratio (Fig. 12b1) is almost constant at a relatively low value (about 2×10^{-6} kg kg^{-1}) before Ls = 210°, and then shows the double-peak episodes of dust lifting events (episodic value about 11×10^{-6} kg kg^{-1}) between Ls = 240° and 320°, and there is a relatively quiet period (about 6×10^{-6} kg kg^{-1}) near the solstice. On the other hand, the time series of low-level dust mixing ratio in RmTerrain (Fig. 12b1, red dashed line) shows a flat curve with a mean value similar to that in CTRL before the dust storm season. Instead of having a double-peak shape of dust events, there is a single peak of weak dust event around Ls = 200° (Fig. 12b1). Unlike the case of low-level dust mixing ratio, in both experiments the double-peak shape can be seen in the time series of

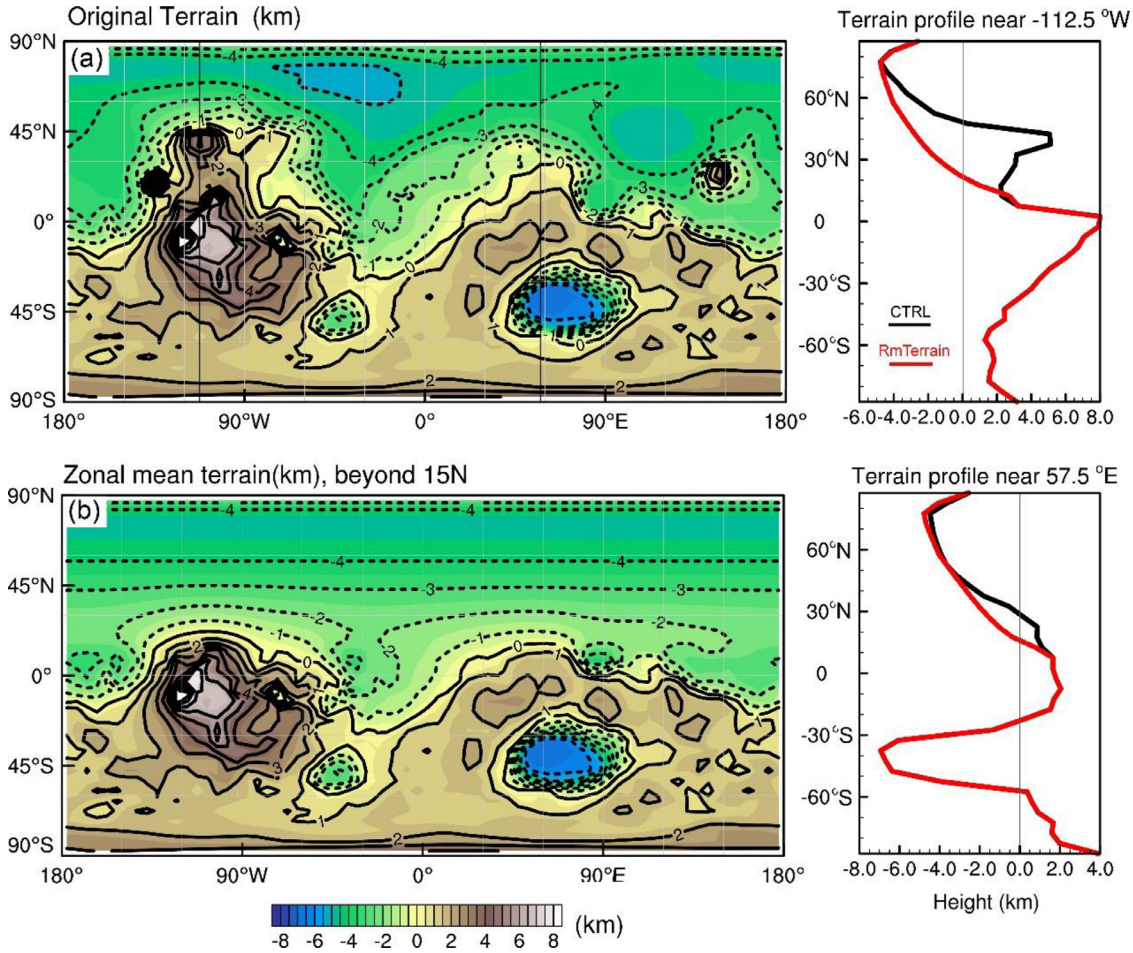

Fig. 11. Topographies in (a) the control experiment (CTRL); and (b) the experiment (RmTerrain) in which zonal-mean terrain is used in latitudes north of 15° N. The curves in the right (black for CTRL and red for RmTerrain) show the profiles of topography near the region of Alba Patera (112.5° W) and the western part of the Hellas Basin (57.5° E). (For interpretation of the references to color in this figure legend, the reader is referred to the web version of this article.)

zonal-mean surface wind stress (Fig. 12b2), except that the magnitude of wind stress in RmTerrain is generally smaller and the "solstice pause" period is longer than that in CTRL. Since the surface wind stress in RmTerrain is generally lower than the dust lifting threshold, dust lifting activities in RmTerrain are substantially reduced.

It has been discussed in Section 3.2 that mid-latitude synoptic waves with typical period about 6 sols is important to the process of dust lifting on the synoptic time scale. It is interesting to investigate whether the high topography in the northern mid-latitude region has important effect on the characteristics of the synoptic waves as well as the dust lifting processes. When the asymmetric topography is smoothed out in RmTerrain experiment, the Hovmöller diagram of the surface wind stress in the northern mid-latitude region still shows significant westward propagating diurnal-scale variations (Fig. 13a). In contrast, without the enhancement of the high terrain, the surface wind maxima can hardly exceed the threshold value for dust lifting. When the diurnal variations are removed, the daily-mean surface wind stress shows the eastward propagating wave signals similar to those in CTRL (c.f. Figs. 9a and 13b).These waves in RmTerrain also have the typical period of 6 to 7 sols in the mid-latitude region. However, without the high topography the amplitudes of the waves are generally weaker except when propagating to the longitude near 120° E where they are strengthened. In the zonal direction, the wave spectrum energy is still dominated by the wave numbers from 2 to 3 during the dust storm season in RmTerrain (Fig. 13c). This feature is similar to that in CTRL except the wave spectrum energy is substantially weaker for higher wave numbers (4 to10) in RmTerrain.

5. Conclusions and discussions

In this study, the dynamical processes of dust lifting at the northern mid-latitude region of Mars during the dust storm season have been investigated. The results in this study are mainly based on numerical simulations performed using the Mars GCM MarsWRF. The GCM adopts an active dust lifting parameterization scheme in which dust lifting is dependent on the surface wind stress, and the effect of dust-radiation interaction in the atmosphere is considered. The simulation results suggest that the GCM is capable of reasonably simulating the regular dust climate on Mars, particularly the double-peak episodes (Ls = 220° - 260° and Ls = 310° - 340°) of dust storm activities during the dust storm season. In these episodic periods, dust storms are frequently initiated in the northern mid-latitude region (40° - 50° N), particularly near the three regions with high terrain (north and downstream of the Alba Patera, north of the Arabia Terra and the Elysium Mountain). The prevailing dust activities in these three regions are generally consistent with some previous observations. In fact, analysis of the simulation results suggests that the dust lifting activities are dominated by a wave-number-three mode in the zonal direction.

The Hovmöller diagrams of low-level dust mixing ratio and surface wind stress suggest that there are basically two types of propagating signals. One is a higher frequency westward signal and the other is a lower frequency eastward signal. Furthermore, by applying wavelet analysis to the time series of the model results, three distinct modes of dust lifting activities with different ranges of period can be identified.

Seasonal mode (period of 50 - 200 sols):

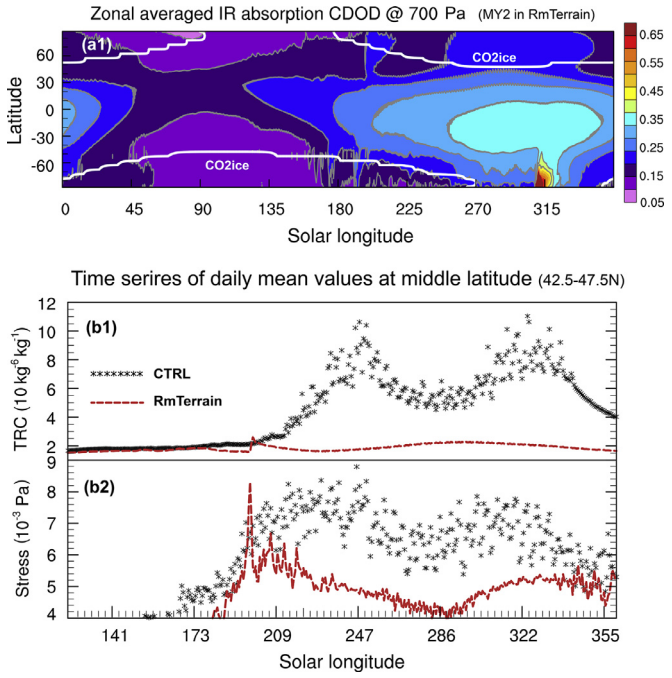

Fig. 12. Results from the experiment RmTerrain. (a) Similar to Fig. 2a but for the experiment RmTerrain. (b1) Time series of daily and zonal mean surface dust mixing ratio (10^{-6} kg kg^{-1}) in CTRL (grey crosses) and RmTerrain (red dashed curves) averaged between 42.5° and 47.5° N. (b2) surface wind stress (10^{-3} Pa). (For interpretation of the references to color in this figure legend, the reader is referred to the web version of this article.)

This mode is basically associated with the seasonal variation in solar radiation over the mid-latitude region, and is responsible to the establishment of the principle westerly wind in the region.

Synoptic mode (period of 3 - 7 sols):

This mode is likely associated with the activities of planetary waves initiated due to barotropic and/or baroclinic instability in the mid-latitude region. The eddies have a primary zonal wave number between 2 to 3 and take 5 to 7 sols to encircle the planet in the mid-latitude region. This mode is basically responsible for the eastward propagating signals in the Hovmöller diagrams.

Diurnal mode (period of 0.5 - 1 sol):

This mode is generally associated with the thermal tides and modulated by topography. Due to the relatively low thermal inertial coefficient of land surfaces, ground temperature increases rapidly near the local noon. This in turn would increase the meridional gradient of the ground temperature, low-level geopotential height and so the surface wind stress north of the region with maximum solar radiation, and finally triggers the occurrence of dust storms if the wind stress exceeds the threshold value. This effect is more significant over the region with high topography, especially near the northern edge and downstream of the Alba Patera. This mode is basically responsible for the westward propagating signals in the Hovmöller diagrams.

For all the above three modes, suppression of dust lifting activities in the solstice period (usually known as solsticial pause) can be observed, but is more significant in the synoptic and diurnal modes. The simulation results suggest that dust lifting activities are mainly caused by the combined effects of the above three modes. Beyond the dust storm season (Ls = 180° - 360°), when the principle zonal wind associated with the seasonal mode is generally absent, the surface stress associated with the synoptic and diurnal modes may not be sufficient for dust lifting. During the dust storm season, dust storms are usually initiated in the areas with high topography where the diurnal mode is significant. However, some time the surface stress associated with this mode alone may still be insufficient for dust lifting, until the constructive contribution of surface stress from the synoptic mode is added in.

Finally, results of sensitivity experiments have confirmed the hypothesis that topography in the northern mid-latitude region (40° - 50° N) is important to the lifting of dust. When the asymmetry in topography is removed for the region north of 15° N, dust lifting activities in the mid-latitude region dramatically decrease and the double-peak episodes basically disappear. The topographical effect is particularly important to intensify the wind stress associated with the thermal tide.

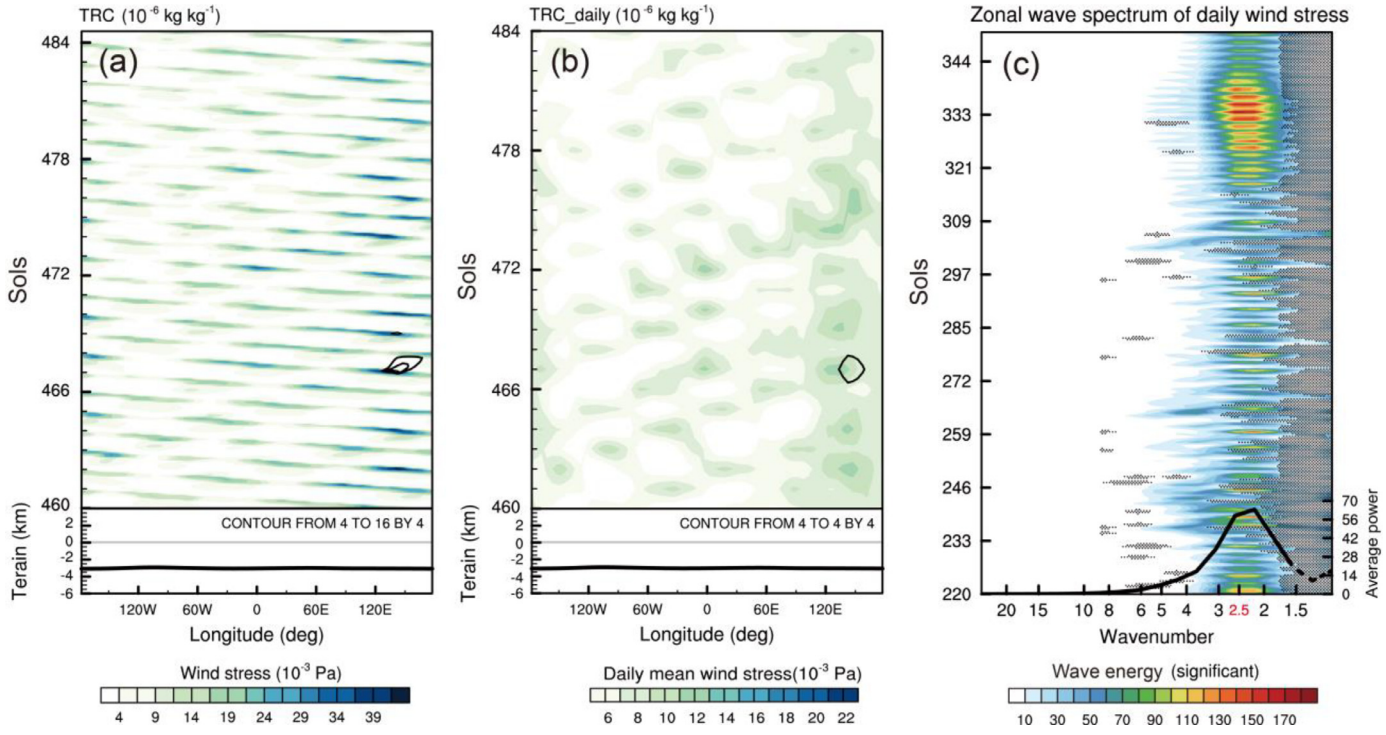

Fig. 13. Time evolution of surface dust mixing ratio and wind stress in RmTerrain experiment. (a) is similar to Fig. 4, and (b)-(c) are similar to Fig. 9.

However, topography may have little impact on the predominant mode of planetary waves.

Acknowledgments

This research is funded by the grants from the FDCT of Macau (grant no. 039/2013/A2 and 080/2015/A3). The data of the numerical simulations, as well as the model codes are freely available from the first author on request. The observational data of column dust optical depth based on Montabone et al. (2015) was obtained from the Laboratoire de Météorologie Dynamique du CNRS (LMD) and is available at http://www-mars.lmd.jussieu.fr/mars/dust_climatology/.

Supplementary materials

Supplementary material associated with this article can be found, in the online version, at doi:10.1016/j.icarus.2018.07.020.

References

Barnes, J.R., 1980. Time spectral analysis of midlatitude disturbances in the Martian atmosphere. J. Atmos. Sci. 37, 2002–2015.
Banfield, D., Coratha, B.J., Gierasch, P.J., et al., 2004. Traveling waves in the Martian atmosphere from MGS TES nadir data. Icarus 170, 365–403.
Basu, S., Wilson, J., Richardson, M.I., et al., 2006. Simulation of spontaneous and variable global dust storms with the GFDL Mars GCM. J. Geophys. Res. (Planets) 111 (E10), 9004. https://doi.org/10.1029/2005JE002660.
Cantor, B.A., James, P.B., Caplinger, M., Wolff, M.J., 2001. Martian dust storms: 1999 Mars Orbiter Camera observations. J. Geophys. Res. 106, 23653–23687.
Chow, K.C., Chan, K.L., Xiao, J., 2018. Dust Activity over the Hellas Basin of Mars during the period of southern spring equinox. Icarus Accepted.
Guo, X., Lawson, W.G., Richardson, M.I., et al., 2009. Fitting the Viking Lander surface pressure cycle with a Mars general circulation model. J. Geophys. Res. 114, E07006. https://doi.org/10.1029/2008JE003302.
Guzewich, S.D., Toigo, A.D., Kulowski, L., Wang, H., 2015. Mars Orbiter Camera climatology of textured dust storms. Icarus 258, 1–13.
Heavens, N.G., McCleese, D.J., Richardson, M.I., et al., 2011. Structure and dynamics of the Martian lower and middle atmosphere as observed by the Mars Climate Sounder: 2. Implications of the thermal structure and aerosol distributions for the mean meridional circulation. J. Geophys. Res. 116, E01010. https://doi.org/10.1029/2010JE003713.
Hinson, D.P., Wilson, R.J., 2002. Transient eddies in the southern hemisphere of Mars. Geophys. Res. Lett. 29. https://doi.org/10.1029/2001GL014103.
Hinson, D.P., Wang, H., 2010. Further observations of regional dust storms and baroclinic eddies in the northern hemisphere of Mars. Icarus 206 (1), 290–305.
Hinson, D.P., Wang, H., Smith, M.D., 2012. A multi-year survey of dynamics near the surface in the northern hemisphere of Mars: Short-period baroclinic waves and dust storms. Icarus 219, 307–320. https://doi.org/10.1016/j.icarus.2012.03.001.
Hollingsworth, J.L., Haberle, R.M., Barnes, et al., 1996. Orographic control of storm zones on Mars. Nature 380, 413–416.
Hollingsworth, J.L., Kahre, M.A., 2010. Extratropical cyclones, frontal waves, and Mars dust: modeling and considerations. Geophys. Res. Lett. 37, L22202. https://doi.org/10.1029/2010GL044262.
Hong, S.Y., Pan, H.L., 1996. Nonlocal boundary layer vertical diffusion in a medium-range forecast model. Mon. Weather Rev. 124 (10), 2322–2339.
Jiménez, P.A., Dudhia, J., González-Rouco, J.F., Navarro, J., Montávez, J.P., García-Bustamante, E., 2012. A revised scheme for the WRF surface layer formulation. Mon. Wea. Rev. 140, 898–918.
Kass, D.M., Kleinbohl, A., McCleese, D.J., et al., 2016. Interannual similarity in the Martian atmosphere during the dust storm season. Geophys. Res. Lett. 43, 6111–6118.
Kavulich Jr., M.J., Szunyogh, I., Gyarmati, G., Wilson, R.J., 2013. Local dynamics of baroclinic waves in the Martian atmosphere. J. Atmos. Sci. 70, 3415–3447. https://doi.org/10.1175/JAS-D-12-0262.1.
Kuroda, T., Medvedev, A.S., Hartogh, P., Takahashi, M., 2007. Seasonal changes of the baroclinic wave activity in the northern hemisphere of Mars simulated with a GCM. Geophys. Res. Lett. 34 (9), L09203. https://doi.org/10.1029/2006GL028816.
Lemmon, M.T., Wolff, M.J., Bell, J.F., et al., 2015. Dust aerosol, clouds, and the atmospheric optical depth record over 5 Mars years of the Mars Exploration Rover mission. Icarus 251, 96–111.
Lewis, S.R., Mulholland, D.P., Read, P.L., et al., 2016. The solsticial pause on Mars: 1. A planetary wave reanalysis. Icarus 264, 456–464. https://doi.org/10.1016/j.icarus.2015.08.039.
Mulholland, D.P., Lewis, S.R., Read, P.L., et al., 2016. The solsticial pause on Mars: 2. Modeling and investigation of causes. Icarus 264, 465–477. https://doi.org/10.1016/j.icarus. 2015.08.038.
McCleese, D.J., Heavens, N.J., Schofield, J.T., et al., 2010. Structure and dynamics of the Martian lower and middle atmosphere as observed by the Mars Climate Sounder: seasonal variations in zonal mean temperature, dust, and water ice aerosols. J. Geophys. Res 115, E12016. https://doi.org/10.1029/2010JE003677.
Montabone, L., Forget, F., Millour, E., et al., 2015. Eight-year climatology of dust optical depth on Mars. Icarus 252, 65–95.
Montabone, L., Marsh, K., Lewis, S.R., et al., 2014. The Mars analysis correction data assimilation (MACDA) dataset V1.0. Geosci. Data J. 1, 129–139. https://doi.org/10.1002/gdj3.13.
Newman, C.E., Richardson, M.I., 2015. The impact of surface dust source exhaustion on the Martian dust cycle, dust storms and interannual variability, as simulated by the MarsWRF general circulation model. Icarus 257, 47–87.
Read, P.L., Lewis, S.R., 2004. The Martian Climate Revisited, Edited by. Springer, Belin.
Read, P.L., Montabone, L., Mulholland, D.P., et al., 2011. Midwinter suppression of baroclinic storm activity on Mars: observations and models. In: Proceedings of the Fourth International Workshop: Mars Atmosphere Modelling and Observations, pp. 8–11 February 2011, Paris, France.
Read, P.L., Lewis, S.R., Mulholland, D.P., 2015. Rep. Progr. Phys. 78 (12), 125901.
Richardson, M.I., Toigo, A.D., Newman, C.E., 2007. PlanetWRF: a general purpose, local to global numerical model for planetary atmospheric and climate dynamics. J. Geophys. Res. 112. https://doi.org/10.1029/2006JE002825.
Skamarock, W.C., Klemp, J.B., 2008. A time-split non-hydrostatic atmospheric model for weather research and forecasting applications. J. Comput. Phys. 227 (7), 3465–3485.
Toigo, A.D., Lee, C., Newman, C.E., et al., 2012. The impact of resolution on the dynamics of the Martian global atmosphere: varying resolution studies with the MarsWRF GCM. Icarus 221 (1), 276–288.
Wang, H., Richardson, M.I., Wilson, R.J., et al., 2003. Cyclones, tides and the origin of major dust storms on Mars. Geophys. Res. Lett. 30 (9), 1488. https://doi.org/10.1029/2002GL016828.
Wang, H., Zurek, R.W., Richardson, M.I., 2005. Relationship between frontal dust storms and transient eddy activity in the northern hemisphere of Mars as observed by Mars Global Surveyor. J. Geophys. Res. 110, E07005. https://doi.org/10.1029/2005JE002423.
Wang, H., 2007. Dust storms originating in the northern hemisphere during the third mapping year of Mars Global Surveyor. Icarus 189, 325–343. https://doi.org/10.1016/j.icarus.2007.01.014.
Wang, H., Richardson, M.I., Toigo, A.D., et al., 2013. Zonal wavenumber three traveling waves in the northern hemisphere of Mars simulated with a general circulation model. Icarus 223, 654–676. https://doi.org/10.1016/j.icarus.2013.01.004.
Wang, H., Richardson, M.I., 2015. The origin, evolution, and trajectory of large dust storms on Mars during Mars years 24–30 (1999–2011). Icarus 251, 112–127. https://doi.org/10.1016/j.icarus.2013.10.033.
Wang, H., Toigo, A.D., 2016. The variability, structure and energy conversion of the northern hemisphere traveling waves simulated in a Mars general circulation model. Icarus 271, 207–221.